ORIGINAL RESEARCH PAPER

Cyanide ion oxidation by catalytic effect of nickel ferrites activated carbon composites

C.Y. Feijoo[1,2,*], E. De la Torre[0], R.A.C. Narváez[2,3]

[1]Department of Extractive Metallurgy, Escuela Politécnica Nacional, Ladrón de Guevara, Quito 170517, Ecuador

[2]Instituto de Investigación Geológico y Energético, Quito, Ecuador

[3]Universidad Central del Ecuador, UCE-GIIP, EC170521, Quito, Ecuador

ARTICLE INFO

ABSTRACT

BACKGROUND AND OBJECTIVES: Cyanide is a commonly-used substance in the gold recovery processes due to its high affinity for forming complexes with the precious metal, but inadequate handling and its final arrangement can lead to severe environmental contamination. In this context, this research focuses on the preparation of nickel ferrite-activated carbon catalysts for catalytic oxidation of cyanide ion in the presence of air.

METHODS: Hydrated salts of nickel ($Ni(NO_3)_2 \cdot 6H_2O$) and iron ($Fe(NO_3)_3 \cdot 9H_2O$) were used as precursors. The preparation pathways of ferrite and of ferrite-activated carbon composites were hydro-chemical with oxalic acid ($C_2H_2O_4$) and co-precipitation with sodium hydroxide. The parameters evaluated for catalyst preparation were Ni/Fe molar ratios (1/1.5 and 1/2), calcination times and temperatures (2-4 h/600-900°C), and ferrite-activated carbon mass ratios in the case of composites (1/1, 1/2 and 1/3).

FINDINGS: Oxidation results showed that the ideal Ni/Fe molar ratio was 1/2, and the calcination time was 4 h at 600 and 900°C for co-precipitation and hydro-chemical pathways of nickel ferrites, respectively. The catalyst that showed the greatest capacity for cyanide transformation was that obtained by the hydro-chemical pathway with oxalic acid, achieving efficiencies of 96.3% oxidation of cyanide ion. It was also determined that the largest impregnation of ferrite on the carbonaceous surface was 52.6% through the treatment with oxalic acid, with which the composite was obtained with the best catalytic properties of cyanide ion.

CONCLUSION: Nickel ferrite is able to oxidize cyanide ion to cyanate ion; being the ferrite-activated carbon combination, with which composite materials with catalytic properties of cyanide ion are obtained. Because of this, the materials studied could be applied in the detoxification of cyanurate solutions from metallurgical processes.

NUMBER OF REFERENCES
38

NUMBER OF FIGURES
10

NUMBER OF TABLES
6

Corresponding Author:
Email: cristhian.feijoo@epn.edu.ec
Phone: +593-9-95506947
Fax: +593-9-95506947

Note: Discussion period for this manuscript open until July 1, 2021 on GJESM website at the "Show Article.

INTRODUCTION

Sodium cyanide (NaCN) is a feedstock widely used in gold extraction through hydro-chemical paths due to their chemical affinity. However, it becomes a significant pollutant when the effluents generated in such metallurgical processes are not handled properly downstream. This is because they cause known impacts to surrounding flora and fauna (Kuyucak and Akcil, 2013). NaCN is also identified as a toxic substance that is capable of generating hydrogen cyanide at pH levels below 9.4 (Stavropoulos *et al.*, 2013). At industrial scale, several processes have been developed and implemented for cyanide removal. Moreover, several water treatment methods add strong oxidizing agents such as hydrogen peroxide (H_2O_2) and Caro's acid ($H_2SO_4+H_2O_2$) in order to counteract the pollutant effect of cyanide. However, both oxidizing agents are usually expensive alternatives that are required in significant amounts (Teixeira *et al.*, 2013a; Teixeira *et al.*, 2013b). The development of effective and recyclable catalysts for the cyanide oxidation process has been a relevant area of development. Several authors have reported suitable alternatives from activated carbon (Halet *et al.,* 2015; Kaušpėdienė *et al.*, 2017; Sivakumar, 2015), metal and activated carbon composites (Pesántez *et al.*, 2010; Singh and Balomajumder, 2016), biomass (Dehghani *et al.*, 2016), blends of iron, nickel, titanium and cobalt oxides (Kadi and Mohamed, 2015), and copper, nickel and cobalt ferrites (De la Torre *et al.*, 2018; Kariim *et al.*, 2020). As part of this trend, ferrite-based magnetic nanoparticles MFe_2O_4 (M: Ni, Zn, Mn, Cu) show several advantages, such as significant saturation magnetization, superparamagnetism, stability under high frequency conditions, and chemical and mechanical durability, among others (Hung and Thanh, 2011). Trevorite, for instance, is a rare type of spinel with a considerable nickel content with the chemical formula $NiFe_2O_4$. This compound is commonly reported in meteorites rather than terrestrial environments (O'Driscoll *et al.*, 2014). Their nanoparticles are reported to have adsorbent properties due to their biocompatibility. Moreover, they are characterised by strong paramagnetism and adsorption capacity, low toxicity and relatively ease of preparation. Inverse spinel structured $NiFe_2O_4$ ferrite shows ferromagnetism originating from the magnetic momentum of antiparallel spins between the Fe^{3+} ions (located in the tetrahedral interstice) and the Ni^{2+} ions (located in the octahedral interstice). $NiFe_2O_4$ ferrite shows a large surface area and low resistance for mass transfer. Moreover, the magnetic behaviour of these nanoparticles is linked to their size (Zandipak and Sobhanardakani, 2016). The most common wet-pathway procedures for ferrite synthesis are thermal decomposition of proper precursors, hydro-chemical solvo synthesis, inverse micelle synthesis, polyol-assisted synthesis, non-aqueous sol-gel and co-precipitation (Diodati *et al.*, 2014; Hajalilou and Mazlan, 2016; Rafique *et al.*, 2016). In this research, two methods for obtaining Nickel ferrite were assayed: co-precipitation with sodium hydroxide and a hydro-chemical synthesis in a dissolution of oxalic acid. These approaches were defined by considering the following information: De la Torre *et al.* (2018) synthesised Copper and Cobalt ferrite composites supported in activated carbon, using Copper, Cobalt and Iron Nitrates. A factor of 2 was adopted for the molar Fe/Cu and Fe/Co ratios. Ferrites were obtained through precipitation with sodium hydroxide at pH levels above 7 through the generation of mixed oxides $NiO \cdot Fe_2O_3$ like the ones presented in Fig. 1. The precipitated compound was supported over activated carbon in 1:1 (mass proportion). Blends were treated at 750°C for 4 hours. The catalysts' effectiveness reached 98% in terms of cyanide oxidation over 8 hours with aeration.

Kadi and Mohamed (2015) prepared a $NiFe_2O_4$/TiO_2-SiO_2 nanocomposite with magnetic properties and catalytic activity for cyanide oxidation. The authors reported assays carried out with several dispersing solutions and oxide ratios. Among these alternatives, $NiFe_2O_4$ preparation at a molar Fe/Ni ratio of 2, 0.1 M oxalic acid as precursor and thermal treatment at 600 °C (Kadi and Mohamed, 2014) delivered the most promising results. Other relevant alternatives were SiO_2/$NiFe_2O_4$, ethanol/$NiFe_2O_4$, NH_3/$NiFe_2O_4$ and Ti/ethanol at 0.03, 20, 1 and 0.8, correspondingly. The synthesized catalyst reported 100% cyanide removal after 1 hour of assay. It is important to mention that ferrites have a low solubility in cyanide solutions due to their refractory properties. The maximum dissolution capacity is approximately 4 % for Copper, Nickel and Cobalt and 1 % for Iron, considering the initial mass of metals (Rojas and Bustamante, 2007). Nickel ferrite ($NiFe_2O_4$) in contact with an aqueous solution of cyanide causes the catalyst to act as a reversible oxygen carrier, which allows the cyanide to
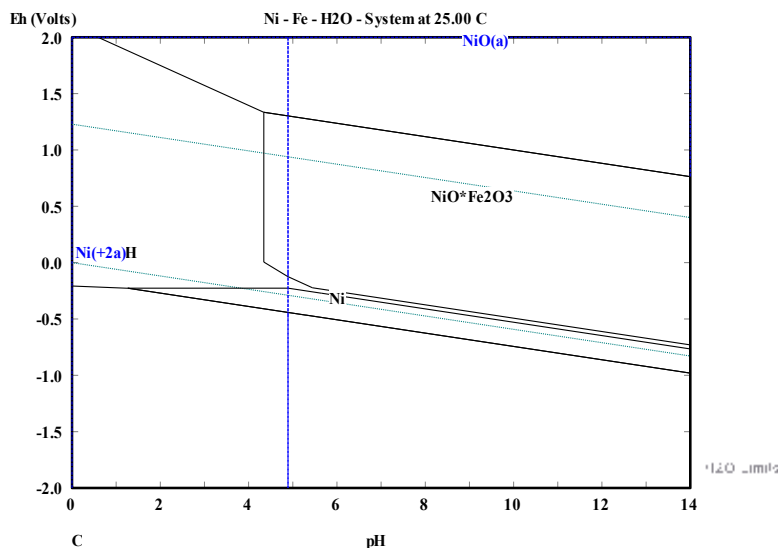
Fig. 1: Eh-pH diagram for Ni-Fe-H$_2$O at 25°C, molar ratio Fe/Ni=2

be oxidized to cyanate. At the same time, the catalyst can be regenerated at the moment it captures oxygen from the air to return to its original state (Kuo *et al.,* 2013). Likewise, activated carbon adsorbs molecular oxygen, which reacts with functional groups to form hydrogen peroxide, and this in turn oxidizes the cyanide ion (De la Torre *et al.,* 2018). In this research, the main objective was the study of the oxidation of cyanide by catalytic action of nickel ferrite-activated carbon composites. For this, it was necessary to evaluate the parameters involved in the preparation of nickel ferrites by both hydro-chemical and co-precipitation pathways, followed by impregnation of these ferrites on granular activated carbon, and catalysts that were evaluated through cyanide oxidation kinetic assays in order to measure their catalytic efficiencies and recyclability in the cyanide solution purification process. The experiments and analysis were done in the extractive metallurgy laboratory of the Escuela Politécnica Nacional (The National Polytechnic University) in Quito, Ecuador in 2019.

MATERIALS AND METHODS

In this research, the preparation of ferrite-based catalysts was through the hydro-chemical pathway with oxalic acid (C$_2$H$_2$O$_4$, analytical grade 98%, Acros Organics) as a precursor and through the co-precipitation pathway with sodium hydroxide (NaOH,

analytical grade 97.0-98.8%, Fisher Scientific).

Nickel ferrites preparation
Hydro-chemical pathway with oxalic acid (OA)

In order to obtain Ni^{+2} and Fe^{+3}, Nickel Nitrate hexa-hydrated (Ni(NO$_3$)$_2$·6H$_2$O, analytical grade 98.5%, Taian Health Chemical Co. Ltd.) and Iron Nitrate nona-hydrated (Fe(NO$_3$)$_3$·9H$_2$O, analytical grade 98.5%, Taian Health Chemical Co. Ltd.) were used. The catalysts' preparation assays were carried out with molar Ni/Fe ratios of 1/1.5 and 1/2. Salts were added to 100 mL of OA at 1 M of concentration. The blending process was performed on a magnetic stirrer hot plate at 300 rpm and 80°C for 3 hours. After this stage, the blends were dried at 110°C for 24 hours. Once the moisture was removed, the samples were taken to an oven for their thermal activation. The process started at ambient temperature and reached 750°C with a heating slope of 12.5°C/min. The maximum temperature was for during 4 hours after it was reached. The remaining soluble compounds were removed through washing. This was done with 100 mL of sulphuric acid at 2% v/v (H$_2$SO$_4$, analytical grade 96.6% w/w, Fisher Scientific). Afterwards, a drying stage (110°C for 12 hours) was included. With the previous tests, once the best Ni/Fe molar ratio was defined, the same one with which the highest oxidation of the cyanide ion was achieved, the conditions of 600, 750 and 900°C were tested to establish the effect of the calcination temperature on

the preparation of ferrites.

Nickel ferrite preparation through the co-precipitation pathway with sodium hydroxide (SH)

This process required the salts to be dissolved in 300 mL of a sodium hydroxide (NaOH) solution 0.4 M with stirring at 500 rpm and ambient temperature. Also, the addition of a basic solution of 20% w/v NaOH was added until a pH level of 7 was reached. The stirring process was applied for 2 hours. Then, the solids were precipitated, filtered, and washed several times with deionized water. The solids had a slurry consistency, and they were dried at 110°C for 24 hours. As it was considered for the hydro-chemical pathway, molar Ni/Fe ratios of 1/1.5 and 1/2 were assayed. The calcination process at 750 °C for 4 hours was also included. Calcinated materials were washed with 100 mL of sulphuric acid at 2% v/v (H_2SO_4, analytical grade 96.6% w/w, Fisher Scientific) and several times with deionized water. Afterwards, a drying stage (110°C for 12 hours) was also included. As in the hydro-chemical pathway, after achieving the best Ni/Fe molar ratio, the effect of the calcination temperature in the preparation of nickel ferrites was evaluated. The evaluated temperatures were 600, 750 and 900°C.

Nickel ferrites characterization

The synthetized materials that were obtained through both pathways were analysed with X-ray diffraction in order to determine their mineralogical phases (Bruker AXS model D8 Advance). Moreover, their elemental composition was determined with X–ray fluorescence (Bruker S8 Tiger).

Cyanide oxidation assays with Nickel ferrites

The cyanide oxidation tests consisted of performing aeration tests (air flow: 180 NL/h) to cyanurated synthetic solutions of fixed volumes (500 mL) of sodium cyanide (500 mg NaCN/L, analytical grade 95.0%, Merck). In addition, each batch included 15 g/L of catalyst and was stirred at 800 rpm for 8 hours. In each elapsed hour, fixed portions of 5 mL of solution were taken. Regarding the experimental conditions, it was carried out at ambient temperature, and a pH level of 10.5 was maintained during the assays by adding NaOH (20% w/v). Cyanide quantification was performed by titration with solutions of Silver Nitrate (4.33 g/L, $AgNO_3$ analytical grade 98.5%,

Fisher Scientific) and Potassium Iodine (KI analytical grade 99.5%, LobaChemie) at 10% w/v as indicator. Likewise, dissolved oxygen was registered with a potentiometer (Central Kagaku Corp model CGS-5).

The oxidation kinetics were adjusted to a first order reaction. With this, it was possible to determine the reaction's kinetic constant. For this, it was necessary to perform a linear adjustment of the natural logarithm of the free cyanide concentration Ln[CN^-] versus time (t), as indicated in Eq. 1.

$$Ln\left[CN^-\right] = Ln\left[CN^-\right]_o - k*t \tag{1}$$

Ferrite/activated carbon catalysts preparation

Once the catalysts' preparation conditions were defined for the hydro-chemical pathway, ferrite: activated carbon (Calgon GRC 20) mass ratios of 1:1, 1:2 and 1:3 were assayed. In a more detailed manner, the corresponding amounts of $Fe(NO_3)_3 \cdot 9H_2O$ y $Ni(NO_3)_2 \cdot 6H_2O$ were dissolved in OA 1 M while adding granular activated carbon Calgon GRC 20 (obtained through physical activation of coconut shell, with specific area of 1058 m^2/g and mesh of 6x12 (1.68 mm – 3.35 mm granulometry, dp_{80}= 2.25 mm). Blends were initially stirred at 400 rpm for 1 hour at ambient temperature and then at 90°C for 2 hours in the second stage. Moisture was removed from composites through drying at 100°C for 24 hours. Soaked carbon was poured in capped cresols prior to thermal activation with the purpose of reducing combustion. The thermal activation started at ambient temperature and continued until conditions reached the ferrite preparation settings. The last stage consisted of washing activated composites with H_2SO_4 at 2% v/v (100 mL), followed by filtration and drying at 110°C for 4 hours. A similar procedure was applied to the catalysts prepared through co-precipitation. In this case, ferrite:carbon mass ratios of 1:1, 1:2 and 1:3 were assayed. Each batch of solids was blended with 300 mL of SH 0.4 M and an additional dissolution of NaOH 20% w/v until a pH level of 7 was reached. The blends were stirred for 1 hour at ambient temperature then heated at 90°C for 2 hours. In the following stage, the solids were precipitated, filtered and washed with deionized water. The following procedures, including drying and thermal activation, were done under the conditions found in the preparation of the ferrite by

co-precipitation that presented the highest oxidation capacities of the cyanide ion.

Catalysts characterization

Chemical characterization of activated carbon-based composites and of activated carbon was performed according to ASTM standards for activated carbon: moisture (Standard Test Method for Moisture in Activated Carbon (ASTM, 2017), volatiles (standard test method for volatile matter content of activated carbon samples (ASTM, 2014), ash and fixed carbon (standard test method for total ash content of activated carbon (ASTM, 2018). Physical characterization of ferrite-activated carbon composites was carried out through scanning electron microscopy (Vega-Tescan microscope equipped with an EDS Bruker X-ray analyser). And the surface area of the porous materials was performed by nitrogen physisorption (Quantachrome NovaWin analyzer).

Cyanide oxidation assays with ferrites: activated carbon catalysts

The composites obtained through both mechanisms were assayed in oxidation tests with the purpose of identifying the one with the most effectiveness. Each assay consisted in adding 15 g/L of catalyst to a fixed volume of 500 mL of NaCN (500 mg/L). Moreover, stirring and aeration was also included (800 rpm and 180 NL/h, correspondingly).

A comparative analysis of the synergy between the obtained ferrite and activated carbon was also proposed. These assays used 15 g/L of activated carbon and the corresponding amount of Nickel ferrite impregnated on activated carbon. 10 mL aliquots were taken to determine the concentration of iron and nickel in solution by Atomic Absorption Spectrometry, in a Perkin Elmer AA300 spectrometer. In addition, a test was carried out using 15 g/L of granular activated carbon and aeration (180 NL/h), to assess the influence of the catalytic action of activated carbon without impregnation (De la Torre *et al.*, 2018). The tests were carried out in duplicate to evaluate the homogeneity/heterogeneity of the composites when they are subjected to the oxidation test, through the calculation of the standard deviation of the cyanide concentration at each sampling point.

Assessing catalyst recyclability

With the composite that presented the highest cyanide conversion, cyanide removal tests were performed with 4 catalyst cycles with the same conditions as indicated above.

RESULTS AND DISCUSSION

Cyanide oxidation by aeration action reaches 27% after 8 h (Fig. 2), but the combination of activated carbon and aeration oxidizes 43% of the initial cyanide. Continuous agitation and aeration cause
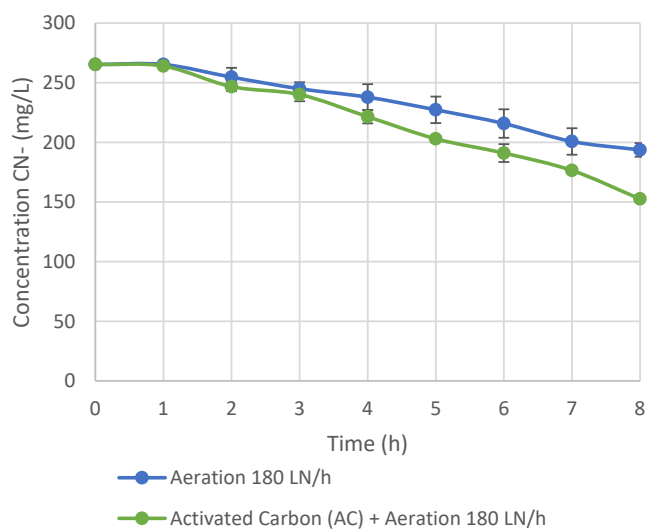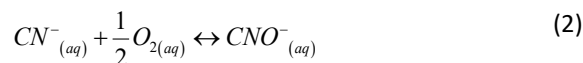

Fig. 2: Cyanide oxidation test with the presence of aeration and with the presence of activated carbon (15 g/L) and aeration, test time 8 h

cyanide ion to react with the supplied oxygen, as indicated in the next reaction Eq. 2 (Chen *et al.*, 2020; Pesántez *et al.*, 2010):

$$CN^-_{(aq)} + \frac{1}{2}O_{2(aq)} \leftrightarrow CNO^-_{(aq)} \qquad (2)$$

On the other hand, the addition of activated carbon (AC) improves cyanide oxidation by 16%, a value that resembles that achieved by Dash *et al.* (2009) of 20% for granular activated carbon's action alone. With the above, the combination AC and aeration is considered able to oxidize twice as much cyanide as only activated carbon (Mudarra, 2017). The carbonaceous surface formed by the different functional groups reacts with molecular oxygen to generate hydrogen peroxide, which acts as an oxidizing agent of cyanide, as indicated in the next reaction Eq. 3 (De la Torre *et al.*, 2018; Tian *et al.*, 2015).

$$CN^-_{(aq)} + H_2O_{2(aq)} \leftrightarrow CNO^-_{(aq)} + H_2O_{(aq)} \qquad (3)$$
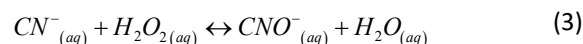
Oxidation of cyanide ion with the use of nickel ferrites

The catalytic action of nickel ferrites ($NiFe_2O_4$) prepared by the two methods, (a) hydro-chemical pathway with oxalic acid (OA) and (b) by co-precipitation pathway with sodium hydroxide (SH), was evaluated. It is important to mention that the hydro-chemical method leads the Ni and Fe ions to meet Ni (+2) and Fe (+3) oxidation states at the moment of coming into contact with the oxalic acid solution, and when the dry mixture remains at high temperatures (600-900ºC), the metals react to form mixed oxide ($NiFe_2O_4$). On the other hand, the preparation by co-precipitation causes the nickel and iron oxides to precipitate with the addition of sodium hydroxide solution, and then in the heat treatment, these reagents react to produce a spinel ($NiFe_2O_4$). With these two explanations, the ferrites obtained differ in their physicochemical, mineralogical, morphological and catalytic properties. That is why in this research, these two methods were evaluated in order to know the preparation conditions at which optimal catalysts for the detoxification of cyanide solutions are obtained.

Table 1 shows the mineral compositions of the different synthesized catalysts, as well as their elemental compositions (iron and nickel). Preliminary preparation of the catalyst by hydro-chemical pathway (OA) with calcination at 600ºC for 2 h (OA R1/2 600-2h) obtains a compound with 44% trevorite (nickel ferrite) and 56% hematite (Fe_2O_3), but with the increase in calcination time to 4 h (OA R1/2 600), the composition of trevorite increases up to 70%. From these tests, it was determined that the optimal calcination time for obtaining nickel ferrites was 4 h. In addition, the influence of the calcination temperature was evaluated. In the case of the OA pathway with a molar Ni/Fe ratio of 1/2 ferrite preparation, by increasing the temperature to 750ºC (OA R1/2 750) while maintaining the calcination time at 4 h, the composition of the ferrite increases by 10%; at 900ºC (OA R1/2 900), it is increased by 8%.

Table 1: X-ray diffraction and x-ray fluorescence analysis of prepared ferrites

Preparation pathway	Theorical Ratio Ni/Fe	Calcination time (h)	Calcination temperature (°C)	Denomination[*]	Trevorite (%)	Hematite (%)	Ni (%)	Fe (%)	Ratio Ni/Fe
Hydro-chemical with oxalic acid	1/2	2	600	OA R1/2 600-2 h	44	56	22.08	52.67	0.42
	1/2		600	OA R1/2 600	70	30	21.21	49.00	0.43
	1/1.5		750	OA R1/1.5 750	82	18	26.17	43.91	0.59
	1/2		750	OA R1/2 750	80	20	19.87	52.56	0.37
	1/2	4	900	OA R1/2 900	78	22	21.41	50.59	0.42
Co-precipitation with sodium hydroxide	1/2		600	SH R1/2 600	99	1	17.87	49.18	0.36
	1/1.5		750	SH R1/1.5 750	99-100	-	23.07	45.89	0.50
	1/2		750	SH R1/2 750	99-100	-	19.06	48.12	0.40
	1/2		900	SH R1/2 900	99-100	-	19.69	49.00	0.40

[*]OA= hydro-chemical pathway with oxalic acid, SH= co-precipitation pathway with sodium hydroxide, R= molar ratio Ni/Fe

When the molar Ni/Fe ratio is 1/1.5 (OA R1/1.5 750), it is only improved by 2% compared to the 1/2 ratio (OA R1/2 750). Additionally, the experimental molar ratio of the samples must range from 0.37 to 0.59, when the theoretical ratio is 0.50. With the cyanide oxidation results shown in Fig. 5, the Ni/Fe ratios are defined, with which the highest efficiencies in the oxidation process are obtained. In the case of the SH pathway, catalysts with at least 99% trevorite were obtained in all preparations, as presented in Table 1, because in the precipitation process at pH greater than 7, mixed nickel and iron oxides were obtained (NiO·Fe$_2$O$_3$), as shown in Fig. 1, according to Zhao *et al.* (2017). The molar ratios obtained ranged from 0.36 to 0.50. It is important to mention that molar ratios deviate from the theoretical value possibly to the dissolution of metals when acidic washing of catalysts was performed, where the color green was observed in the washing solutions. This phenomenon occurs due to the dissolution of nickel and iron oxides (De la Torre *et al.*, 2018).

The XRD patterns in Fig. 3 corresponding to the ferrites prepared by the hydro-chemical pathway show the presence of trevorite (NiFe$_2$O$_4$, nickel ferrite or nickel spinel) and hematite (Fe$_2$O$_3$). The characteristic peaks for trevorite are located at
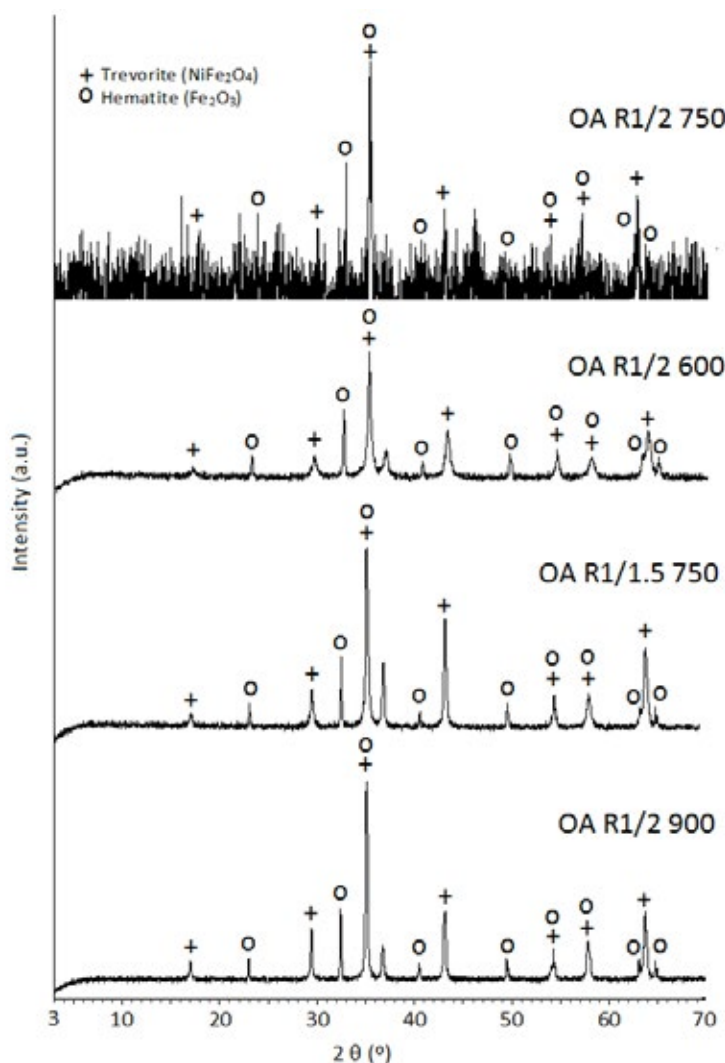

Fig. 3: XRD pattern of ferrites prepared by the hydro-chemical pathway

positions 18.37° (111), 30.28° (220), 35.66° (311), 43.31° (400), 53.78° (422), 57.34° (511) and 62.93° (440) (Livani *et al.*, 2018), and for hematite they are 24.14° (012), 33.24° (104), 35.61° (110), 40.81° (113), 49.47° (024), 54.09° (116), 57.62° (018), 62.46° (214) and 64.13° (300) (Basavegowda *et al.*, 2017). On the other hand, in the case of the ferrites prepared by the co-precipitation pathway (Fig. 4), all the XRD patterns present only trevorite peaks, which is why ferrites with purities greater than 99% are obtained.

With the catalysts shown in Table 1, cyanide oxidation tests were conducted to assess cyanide efficiency, with the results shown in Fig. 5A and 5B. Fig. 5A shows that OA R1/2 600-2h has a lower catalytic action than the other catalysts. This may be because this ferrite has the lowest percentage of trevorite. OA R1/1.5 750 has a linear trend, achieving

an efficiency of 78% at the end of 8 h, whereas its similar OA R1/2 750 has a high oxidation capacity, achieving values like OA R1/1.5 750 in less than 3 h. In Fig. 5B, the catalyst with the least cyanide oxidation capacity is SH R1/2 750 unwashed, due to the presence of sodium that was not completely eliminated in chemical preparation and causes a ferrite with an amorphous structure to be obtained, which in turn is not active (Livani *et al.*, 2018). SH R1/1.5 750 had an efficiency of 56%, but its similar SH R1/2 750 reached 64% oxidation. From the results of Fig. 5, it is confirmed that with a Ni/Fe molar ratio of 1/2, a nickel ferrite is achieved with a crystalline structure with the highest catalysis capacities of the cyanide ion. In conclusion, it was confirmed that the best Ni/Fe ratio was 1/2 for both methods, which achieves the highest yield of nickel ferrite production
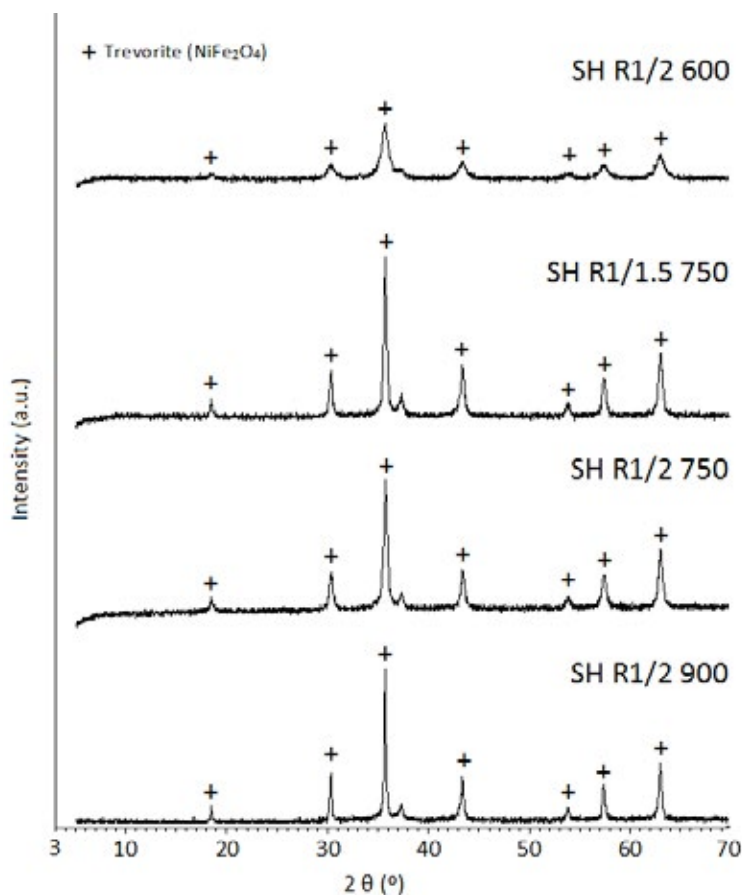

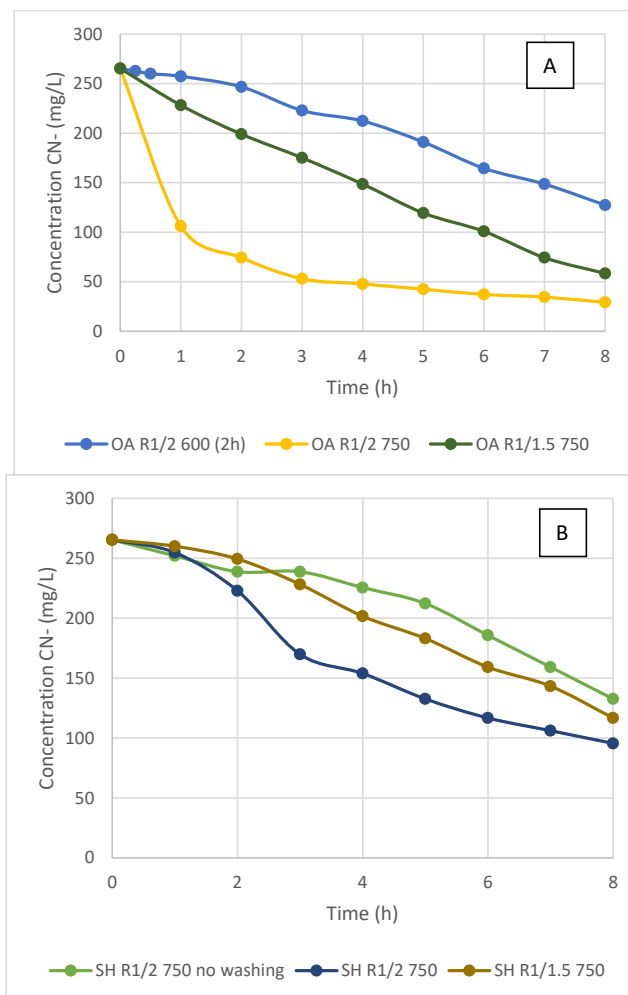Fig. 4: XRD pattern of ferrites prepared by the co-precipitation pathway

Fig. 5: Evaluation of the molar Ni/Fe ratio of ferrites prepared in the oxidation of cyanide ion (15 g/L, 180 NL/h, 5.5-8.5 mg O_2/L, 800 rpm). (a) Hydro-chemical pathway with oxalic acid (OA). (b) Co-precipitation pathway with sodium hydroxide (SH)

and higher oxidation of cyanide ion (Diodati *et al.,* 2014).

To understand the behavior of the curves presented in the graphs of Fig. 5, the kinetic constants and their reaction rates were determined, values that are indicated in Table 2. As can be seen, the kinetics of the reactions conform to a pseudo-first-order, as indicated by some authors who carried out the oxidation of cyanide with the use of ferrites (Guo *et al.,* 2018; Stoyanova and Christoskova, 2005). In the case of the hydro-chemical pathway, when evaluating the Ni/Fe ratio in the preparation of the catalyst, the ratio 1/2 (AO R1/2 750) is that with which a higher reaction rate is achieved and in turn the higher

kinetic constant, in compared to the ratio 1/1.5 (AO R1/1.5 750). The same phenomenon occurs when comparing the reaction rates of the ferrites obtained by the co-precipitation pathway (SH R1/2 750 and SH R1/1.5 750), where the Ni/Fe ratio of 1/2 presents the highest reaction rate and the highest oxidation capacity of the cyanide ion.

From the results of Fig. 5, the influence of calcination temperature was assessed, as shown in Fig. 6A and 6B. In Fig. 6A, at a calcination temperature of 600ºC, the compound OA R1/2 600 presented an efficient oxidation of cyanide after 1 h, after which the curve's trend becomes linear, achieving an efficiency of 85% at the end of 8 h.

At 750°C ferrite calcination, OA R1/2 750 achieves high oxidations until the third hour, after which the cyanide concentration remains almost constant with an efficiency of 89% at 8 h. Finally, the catalyst OA R1/2 900 obtained at 900°C had the highest catalytic activity among all the materials studied (95%), and therefore the higher cyanide oxidation reaction rate compared to the other catalysts, as indicated in Table 2. It is notable to see that, with the increase in the calcination temperature in the hydro-chemical preparation, the catalytic properties of ferrites were improved. In contrast, the co-precipitation pathway at the calcination temperature of 600°C achieved the catalyst SH R1/2 600 with greater oxidation efficiency of cyanide ion. On the other hand, with a heat treatment at 750°C (SH R1/2 750), ferrite decreases its catalytic capacity by 26%, compared to SH R1/2 600. Finally, with a calcination at 900°C, SH R1/2 900 showed the least catalytic activity, reaching a balance at the fourth hour. The catalytic activity of ferrites is based on the Mars-Van Krevelen redox cycle, where an oxygen atom migrates from the catalyst crystal network to the surface to be absorbed by cyanide and the oxidation reaction occurs; then, an oxygen from the aerated liquid phase replaces the vacancy from the migrated atom (Hirabayashi *et al.*, 2006; Kuo *et al.*, 2013). It was determined that the calcination temperature for optimal ferrite obtention by OA hydro-chemical pathway was 900°C, and for the SH co-precipitation pathway it was 600°C. At these temperatures, the impregnation tests of nickel ferrites on granular activated carbon were performed.

Oxidation of cyanide ion with the use of ferrite/activated carbon composites

Fig. 7A and 7B show the oxidation kinetics of cyanide ion with the use of nickel ferrite-activated carbon composites obtained by the two methodologies. The catalyst prepared with a 1/1 mass ratio of ferrite by hydro-chemical pathway OA and activated carbon (R1/1 OA) had the highest catalytic capacity, with oxidation percentages of 96.3% (Table 4). From the proximate analysis it is observed that this compound contains the highest proportion of ash (52.56%, Table 3), equivalent to the ferrite impregnated on the surface of the carbon, so its oxidizing action was the highest reported, compared to the ratios 1/2 (R1/2 OA) and 1/3 (R1/3 OA). It is also evidenced that the mechanism of Mars-Van Krevelen takes place, where the oxygens of the ferrite migrate to the surface of the cyanide ion and achieve oxidation to ion cyanate (Hirabayashi *et al.*, 2006; Manova *et al.*, 2011).

It is estimated that approximately 4% of free cyanide formed complexes with dissolved nickel and iron during oxidation tests, which helps to understand that at least 92% effectively corresponds to the catalytic action of the composite in the oxidation of cyanide. The composite R1/2 OA, despite having 3% more ash content than R1/3 OA, showed a lower reaction rate than the latter (Table 4).

Fig. 7B shows the curves of the cyanide concentration over time through oxidation tests using catalysts of activated carbon impregnated with nickel ferrite prepared by the co-precipitation pathway. In all cases, it is observed that the final

Table 2: Parameters of the reaction kinetics of the prepared catalysts

| Preparation pathway	Catalyst	Kinetic constant k (h⁻¹)	Correlation coefficient (R²)	Reaction Rate (mg/ L·h)	Cyanide oxidation (%)
-	Activated carbon	0.068	0.959	14.09	42.5
Hydro-chemical with oxalic acid	OA R1/2 600	0.197	0.937	28.19	85.0
	OA R1/1.5 750	0.186	0.981	25.87	78.0
	OA R1/2 750	0.230	0.832	29.52	89.0
	OA R1/2 900	0.345	0.979	31.51	95.0
Co-precipitation with sodium hydroxide	SH R1/2 600	0.249	0.965	29.85	90.0
	SH R1/1.5 750	0.103	0.957	18.57	56.0
	SH R1/2 750	0.138	0.983	21.22	64.0
	SH R1/2 900	0.056	0.741	13.27	40.0
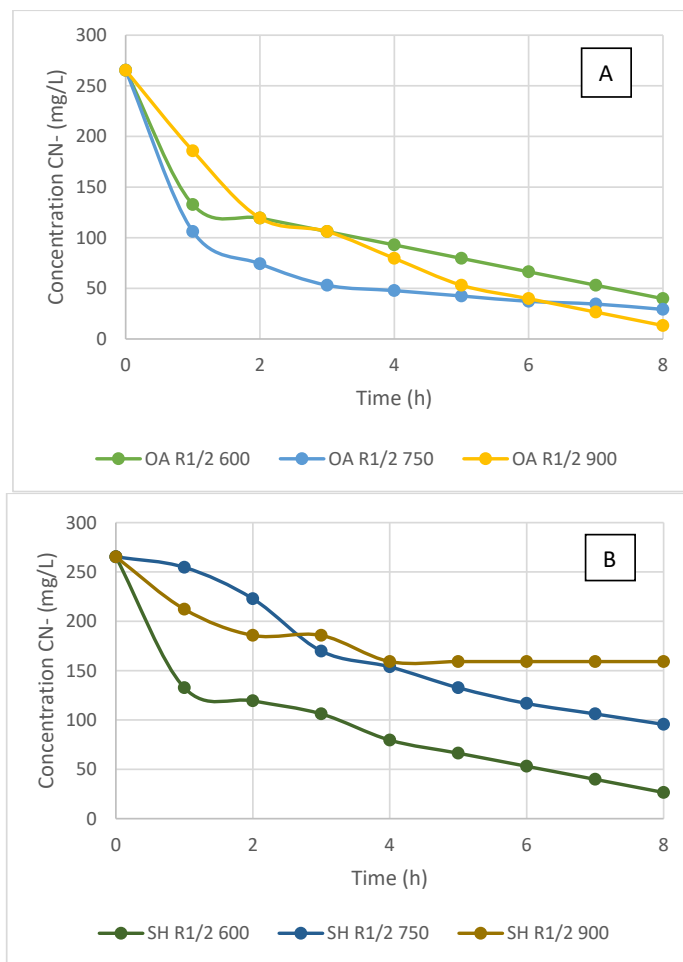
Fig. 6: Influence of the calcination temperature of prepared ferrites on the oxidation of cyanide ion (15 g/L, 180 NL/h, 5.5-8.5 mg O_2/L, 800 rpm). (a) Hydro-chemical pathway with oxalic acid (OA). (b) Co-precipitation with sodium hydroxide (SH)

concentration of cyanide (in the range of 139.3-152.6 mg/L) at the end of 8 h is similar for the 3 composites; so their reaction rates and kinetic constants have similar values (Table 4). Because the impregnations of ferrite by the co-precipitation pathway were less than 18.7%, the prepared composites do not have a good catalysis capacity of cyanide, which resembles that of activated carbon without impregnation. At the time of the calcination of the metal precipitate on the carbonaceous surface, the ferrite cannot be impregnated in a homogeneous manner, and the metal oxides formed agglomerates, which can be separated with the application of a magnetic field. The largest addition of nickel and iron achieved for these composite materials was 2.66% and 5.15%,

respectively. On the other hand, in the case of OA composites, the salts used in impregnation manage to adhere by covering all the grains of the activated carbon, and at the time of calcination, the catalytic materials had greater affinity with the surface of the activated carbon.

Assessment of the recyclability of the ferrite/activated carbon composite

The reuse of the R1/1 OA composite was evaluated, as shown in Fig. 8A, as it is considered the composite with the highest percentage of cyanide ion oxidation. The initial composite showed a catalytic activity of 96%, and after the 4 consecutive cycles, it was 95, 90, 80 and 70%. One of the factors for the
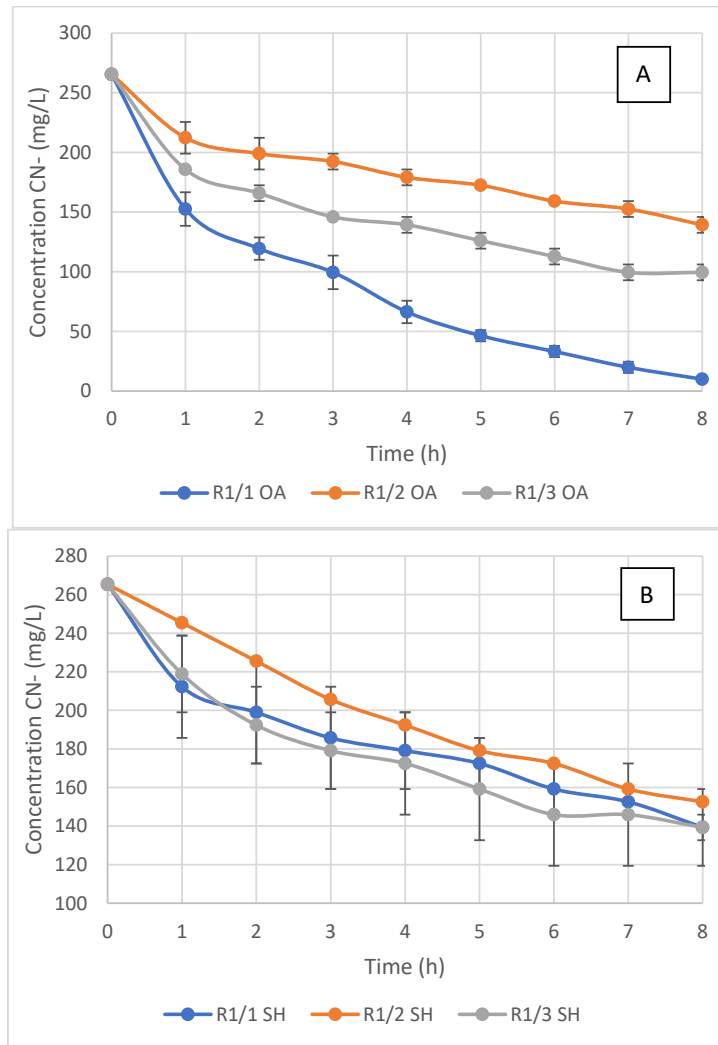
Fig. 7: Evaluation of the mass ratio nickel ferrite/activated carbon (Ratios 1/1, 1/2 and 1/3) in the preparation of catalysts and their influence on the oxidation of cyanide ion (15 g/L, 180 NL/h, 5.5-8.5 mg O_2/L, 800 rpm). (a) by hydro-chemical pathway (OA). (b) by co-precipitation pathway (SH)

Table 3: Proximate analysis of the composites obtained

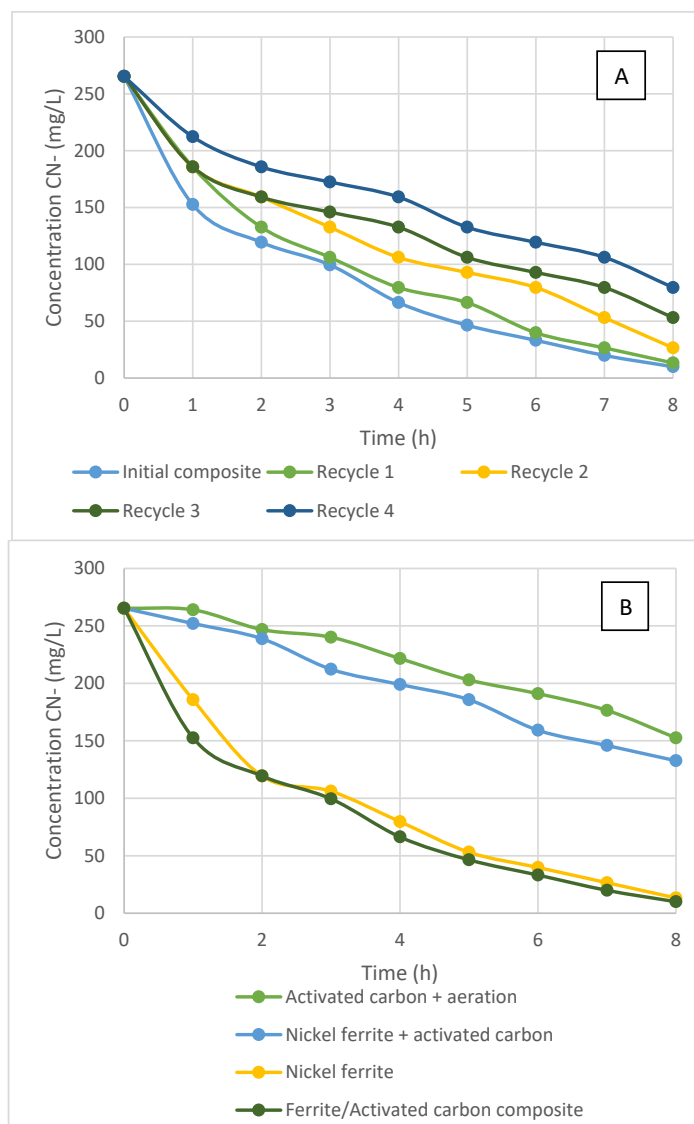| Catalyst	Preparation pathway	Calcination temperature (°C)	Theorical mass ratio NiFe$_2$O$_4$/AC	Real mass ratio NiFe$_2$O$_4$/AC	Molar ratio Ni/Fe	Moisture (%)	Volatiles (%)	Ashes (%)	Fixed carbon (%)
Activated carbon	-	-	-	-	-	6.82	5.79	1.36	92.85
R1/1 OA	Hydro-		1/1	1/0.9	0.61	1.82	10.57	52.56	36.88
R1/2 OA	chemical	900	1/2	1/4.8	0.47	2.15	7.87	17.65	74.48
R1/3 OA	(OA)		1/3	1/5.9	0.63	2.11	8.06	14.82	77.12
R1/1 SH	Co-		1/1	1/4.3	0.49	4.99	10.99	18.72	70.29
R1/2 SH	precipitation	600	1/2	1/100	1.11	3.02	6.39	1.44	92.18
R1/3 SH	(SH)		1/3	1/50	0.66	2.02	6.45	2.17	91.38

Fig. 8: Cyanide oxidation kinetics. (a) Recyclability tests of the R1/1 OA composite, (b) Comparison of catalysts studied. (15 g/L, 180 NL/h, 5.5-8.5 mg O_2/L, 800 rpm)

Table 4: Parameters of the reaction kinetics of the prepared composites

Catalyst	Preparation pathway	Kinetic constant k (h^{-1})	Correlation coefficient (R^2)	Reaction rate (mg/ L·h)	Cyanide oxidation (%)
R1/1 AO		0.419	0.974	32.22	96.3
R1/2 AO	Hydro-chemical (OA)	0.112	0.929	15.75	47.5
R1/3 AO		0.069	0.943	20.73	62.5
R1/1 SH		0.068	0.935	15.75	47.5
R1/2 SH	Co-precipitation (SH)	0.070	0.990	14.09	42.5
R1/3 SH		0.074	0.924	15.75	47.5

Table 5: Comparison of the oxidation capacities of the cyanide ion of different catalysts

Catalyst	Preparation	Cyanide oxidation (%)	Reference
Nickel ferrite ($NiFe_2O_4$)	Co-precipitation	85	Stoyanova and Christoskova, 2005
$NiFe_2O_4$/TiO_2-SiO_2 core-shell nanocomposite	Hydro-chemical	100	Kadi and Mohamed, 2015
Nickel ferrite (OA R1/2 900)	Hydro-chemical	95	This study
Nickel ferrite (SH R1/2 600)	Co-precipitation	90	This study
Nickel ferrite-activated carbon composite (R1/1 OA)	Hydro-chemical	96	This study

Table 6: Surface area BET, volume and pore diameter of the materials studied

Parameter	Calgon Activated Carbon	R1/1 OA	R1/1 SH
Surface area (m^2/g)	1058	610	1008
Volume pore (cm^3/g)	0.77	0.48	0.68
Radius pore (Å)	1.83	1.84	1.84
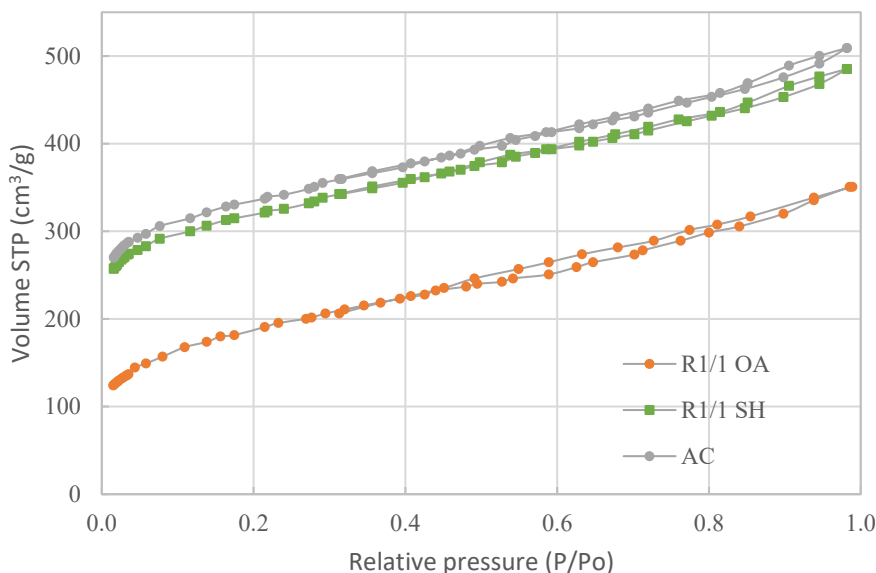
Fig. 9: N_2 adsorption-desorption isotherms of activated carbon and composites

catalytic activity decrease is that during agitation, some of the nickel dissolves in the cyanurate solution, with values ranging from 2.58, 0.92, 0.83, 0.52 and 0.31% Ni, corresponding to the cycles performed; on the other hand, the iron dissolved was less than 0.08% in all tests. The composites are also prone to erosion due to attrition during agitation (Marsden and House, 2006). When comparing the initial composite with the first cycle, it is observed that similar oxidation efficiencies were obtained, making it possible to

assume that the dissolution of nickel does not contribute to the oxidation of cyanide. In addition, a comparative analysis was performed between the R1/1 OA, activated carbon (AC), ferrite ($NiFe_2O_4$) and the activated carbon and nickel ferrite mixture without impregnation, as shown in Fig. 8B. For this, the amount of nickel ferrite was taken from the ash percentage of R1/1 OA and the remaining amount corresponded to the AC. Activated carbon with aeration had the least catalytic action. Nickel ferrite
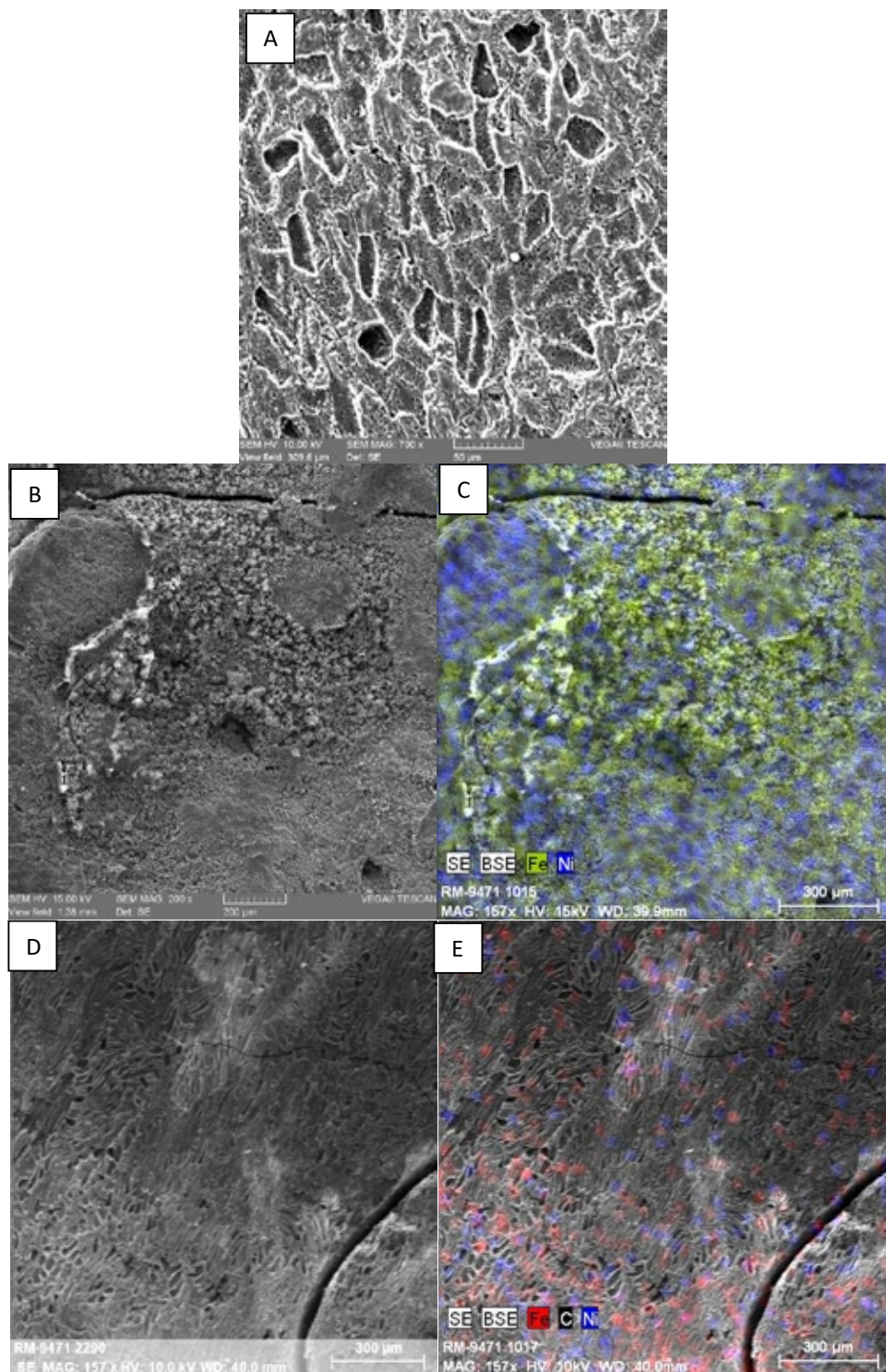
Fig. 10: Scanning electron microscopy images. (a) Activated carbon 700X, Composite R1/1 OA 157X: (b) morphological analysis, (c) elemental analysis by EDS, Composite R1/1 SH 157X: (d) morphological analysis, (e) elemental analysis by EDS

has a kinetics similar to the R1/1 OA composite. Also, it is observed that the AC and ferrite mixture without impregnation had lower oxidation capacity of cyanide compared to the composite, which makes it possible to show that the incorporation of the catalyst on the carbonaceous surface improves catalysis properties, as determined by De la Torre *et al.* (2018).

Table 5 shows a comparison of different nickel ferrite-based catalysts used in the oxidation of the cyanide ion. The nickel ferrite of this study obtained by the co-precipitation method has a higher oxidation capacity than that obtained by Stoyanova and Christoskova (2005). In this study, when working with calcination temperatures of 900°C, ferrites are obtained with a crystalline lattice with greater catalytic capacities than that obtained at 120°C by the mentioned authors. On the other hand, the core-shell nanocomposite (NiFe$_2$O$_4$/TiO$_2$-SiO$_2$) obtained by Kadi and Mohamed (2015) is capable of oxidizing 100% of the initial cyanide. This research achieves a similar value (95%) to that of the second mentioned authors.

From the comparative analyzes indicated, it is established that for this study, the catalyst that presented the best catalytic capacities was the composite of nickel ferrite impregnated in activated carbon, a material prepared by the hydro-chemical pathway in the medium of oxalic acid, Ni/Fe molar ratio of 1/2, calcination temperature of 900°C and ferrite-activated carbon mass ratio of 1/1. This catalyst was able to oxidize more than 96% of the initial cyanide ion, with a reaction rate of cyanide consumption of 32.22 mg/L/h and with a reaction kinetic constant of 0.419 h^{-1} (6.98x10^3/min).

Characterization of the composites

Table 6 shows the results obtained from nitrogen physisorption of activated carbon and prepared composites. Calgon activated carbon has the largest surface area. Following is R1/1 SH, a material that, having a higher proportion of fixed carbon and low impregnated ferrite content, has a porous surface that is not as affected. In contrast, R1/1 OA reduces its surface area by 42.3% compared to unimpregnated carbon, a percentage affected by the incorporation of calcined ferrite into the carbonaceous surface. In all cases, the pore radius is the same, so the pore size is not affected in the impregnation of nickel ferrites.

The nitrogen adsorption and desorption isotherms shown in Fig. 9, indicate that the 3 catalysts fit the type IV isotherms, according to the IUPAC classification, characteristic of mesoporous samples (*Li et al.*, 2017). In the case of the ferrite-carbon composite obtained by the co-precipitation method, the isotherms are similar to those of activated carbon, because this material does not manage to impregnate significant amounts of ferrite on the carbonaceous matrix and therefore, it is not seen to be affected the surface area of activated carbon. On the other hand, in the case of the composite prepared by the hydro-chemical pathway, due to the fact that significant amounts of ferrite are incorporated on the activated carbon, the carbonaceous surface is affected when the pores are closed by the presence of impregnated ferrite. Therefore, this last composite has a lower adsorption capacity; however, its catalytic properties of the cyanide ion are not altered by this phenomenon.

Through scanning electron microscopy analysis, the commercial Calgon carbon has a heterogeneous surface (Fig. 10A), from 700x magnification, the characteristic porosity begins to be observed, indicating a porous material. The R1/1 OA composite (Fig. 10C) shows homogeneity of the metals incorporated into the carbon surface. Also, it was found that in carbon fractures and slits, there are fragments of sintered ferrite as indicated by De La Torre *et al.* (2018). Finally, in R1/1 SH (Fig. 10E), mixed oxide is impregnated in parts where there is no porosity, so it is possible to observe macropores.

CONCLUSION

Nickel ferrites (NiFe$_2$O$_4$) synthesized by hydro-chemical and co-precipitation pathways had catalytic activity of oxidation of cyanide ion to cyanate. Mixed iron and nickel oxides with approximately 100% purity were obtained by the co-precipitation pathway with sodium hydroxide with oxidation efficiencies of 90%. It is important to mention that for this method, it is advisable to carry out several washes with water after the precipitation process in order to obtain ferrites with a high content of the pure species. On the other hand, by preparing the hydro-chemical pathway with oxalic acid, ferrites of 80% purity and oxidation efficiencies of 95% were obtained. These ferrites, due to their crystallization nature, presented the best catalytic oxidation activities of cyanide ion. The purity of these ferrites could be increased by varying the concentration of

oxalic acid when the process of dissolving nickel and iron salts is carried out; also, another influencing factor would be the increase in the calcination temperature during the heat treatment. Activated carbon and nickel ferrite composites were obtained. The hydro-chemical pathway achieved the highest impregnation of mixed nickel and iron oxide, with a maximum value reaching 52.6%; in contrast, with chemical preparation by co-precipitation, the maximum impregnation was 18.7%. This shows that ferrite/activated carbon composites obtained by hydro-chemical preparation with oxalic acid had the best catalytic properties of cyanide oxidation, with reported efficiencies of 96.3%. It should be taken into account that, during the calcination process, the salts and activated carbon mixture must be in covered or insulated containers in order to reduce the losses of carbonaceous material produced by combustion with the oxygen in the environment. Furthermore, recyclability tests of the nickel ferrite-activated carbon composite demonstrate that catalysts have high cyanide oxidation efficiencies (above 70%), but in each cycle, the catalyst loses effectiveness due to the deactivation of the ferrite crystalline structure. There is a noticeable difference when comparing the efficiency of the nickel ferrite catalyst impregnated in activated carbon to the ferrite and carbon mixture without impregnation, where the composite material has twice the catalytic capacity of cyanide ion than the mixture of ferrite and carbon without impregnation. Also, it is beneficial to produce composite-type catalysts as they are easy to handle, recover by sieving or magnetism, and are reusable. Moreover, the scanning electron microscopy of the composites showed uniformity in the distribution of nickel and iron metals on the surface of activated carbon grains, and it was also shown that catalyst fragments occupied the slits of the absorbent material. The materials studied are the basis for the search for new catalysts for the detoxification of cyanurate solutions produced in the mining industry.

AUTHOR CONTRIBUTIONS

C.Y. Feijoo performed the literature review, developed the experiments, analyzed and interpreted the data, prepared the manuscript text, and manuscript edition. E. De la Torre performed the literature review, designed the experiments, compiled the data and manuscript preparation. R.A.C. Narváez helped in the literature review and manuscript preparation.

CONFLICT OF INTEREST

The authors declare no potential conflict of interest regarding the publication of this work. In addition, the ethical issues including plagiarism, informed consent, misconduct, data fabrication and, or falsification, double publication and, or submission, and redundancy have been completely witnessed by the authors.

ABBREVIATIONS

$\mathring{A}$	Armstrong
AC	Activated carbon
°C	Celsius degrees
$C_2H_2O_4$	Oxalic acid
Co	Cobalt
Cu	Copper
CN^-	Cyanide ion
CNO^-	Cyanate ion
dp_{80}	Particle diameter with 80% of the accumulated through-hole
Eh	Redox potential
Fe	Iron
Fe_2O_3	Hematite
$Fe(NO_3)_3 \cdot 9H_2O$	Iron nitrate nona-hydrate
h	Hour
H_2O	Water
H_2O_2	Hydrogen peroxide
H_2SO_4	Sulfuric acid
k	Reaction kinetic constant
L	Liter
m^2	Square meters
M	Metal

MFe₂O₄	Metal ferrite with oxidation state +2
mg	Milligrams
min	Minutes
mL	Milliliters
mm	Millimeters
Mn	Manganese
NaCN	Sodium cyanide
NaOH	Sodium hydroxide
NH₃	Ammonia
Ni	Nickel
NiFe₂O₄	Nickel ferrite/Trevorite
Ni(NO₃)₂·6H₂O	Nickel nitrate hexa-hydrate
NiO	Nickel oxide
NL	Normal liters
O₂	Oxygen
OA	Hydro-chemical pathway with oxalic acid
OA R1/2 600	Nickel ferrite prepared by hydro-chemical pathway, molar Ni/Fe ratio of 1/2, 600ºC temperature and 4 h calcination
OA R1/2 600-2h	Nickel ferrite prepared by hydro-chemical pathway, molar Ni/Fe ratio of 1/2, 600ºC temperature and 2 h calcination
OA R1/1.5 750	Nickel ferrite prepared by hydro-chemical pathway, molar Ni/Fe ratio of 1/1.5, 750ºC temperature and 4 h calcination
OA R1/2 750	Nickel ferrite prepared by hydro-chemical pathway, molar Ni/Fe ratio of 1/2, 750ºC temperature and 4 h calcination
OA R1/2 900	Nickel ferrite prepared by hydro-chemical pathway, molar Ni/Fe ratio of 1/2, 900ºC temperature and 4 h calcination
pH	Hydrogen potential
R1/i OA	Nickel ferrite-activated carbon composite prepared by hydro-chemical pathway, ferrite-carbon mass ratio of 1/i (i=1, 2 or 3)
R1/i SH	Nickel ferrite-activated carbon composite prepared by co-precipitation pathway, ferrite-carbon mass ratio of 1/i (i=1, 2 or 3)
rpm	Revolutions per minute
SH	Co-precipitation pathway with sodium hydroxide

SH R1/2 600	Nickel ferrite prepared by co-precipitation pathway, molar ratio Ni/Fe of 1/2, 600ºC temperature and 4 h calcination
SH R1/1.5 750	Nickel ferrite prepared by co-precipitation pathway, molar ratio Ni/Fe of 1/1.5, 750ºC temperature and 4 h calcination
SH R1/2 750	Nickel ferrite prepared by co-precipitation pathway, molar ratio Ni/Fe of 1/2, 750ºC temperature and 4 h calcination
SH R1/2 900	Nickel ferrite prepared by co-precipitation pathway, molar ratio Ni/Fe of 1/2, 900ºC temperature and 4 h calcination
SiO₂	Silica
Ti	Titanium
TiO₂	Titanium oxide
%	Percentage
%w/v	Percentage weight/volume
Zn	Zinc

REFERENCES

ASTM, (2014). Standard test method for volatile matter content of activated carbon samples. D5832-98. ASTM International.

ASTM, (2017). Standard test method for moisture in activated carbon. D2867-17. ASTM International.

ASTM, (2018). Standard test method for total ash content of activated carbon. D2866-11. ASTM International.

Basavegowda, N.; Mishra, K.; Lee, Y.R., (2017). Synthesis, characterization, and catalytic applications of hematite (α-Fe2O3) nanoparticles as reusable nanocatalyst. Adv. Nat. Sci: Nanosci. Nanotechnol., 8(2): 025017 **(7 pages).**

Chen, Y.; Song, Y.; Chen, Y.; Zhang, X.; Lan, X., (2020). Comparative experimental study on the harmless treatment of cyanide tailings through slurry electrolysis. Sep. Purif. Technol., 251: 117314 **(9 pages).**

Dash, R.; Balomajumder, C.; Kumar, A., (2009). Removal of cyanide from water and wastewater using granular activated carbon. Chem. Eng. J., 146(3): 408-413 **(6 pages)**.

De la Torre, E.; Lozada, A.; Adatty, M.; Gámez, S., (2018). Activated carbon-spinels composites for Waste Water Treatment. Metals, 8(12) **(12 pages)**.

Dehghani, R.; Moosavi, G.; Takhtfiroozeh, S. M.; Rashedi, G., (2016). Investigation of the removal of cyanide from aqueous solutions using biomass Saccharomyces cerevisiae. Desalin. Water Treat., 57(56): 27349-27354 **(6 pages).**

Diodati, S.; Pandolfo, L.; Caneschi, A.; Gialanella, S.; Gross, S., (2014). Green and low temperature synthesis of nanocrystalline transition metal ferrites by simple wet chemistry routes. Nano Res., 7(7): 1027-1042 **(16 pages)**.

Guo, T.; Dang, C.; Tian, S.; Wang, Y.; Cao, D.; Gong, Y.; Zhao,

S.; Mao, R.; Yang, B.; Zhao, X., (2018). Persulfate enhanced photoelectrocatalytic degradation of cyanide using a CuFe2O4 modified graphite felt cathode. Chem. Eng. J., 347: 535-542 **(8 pages).**

Hajalilou, A.; Mazlan, S.A., (2016). A review on preparation techniques for synthesis of nanocrystalline soft magnetic ferrites and investigation on the effects of microstructure features on magnetic properties. Appl. Phys. A, 122(7) **(15 pages)**.

Halet, F.; Yeddou, A. R.; Chergui, A.; Chergui, S.; Nadjemi, B.; Ould-Dris, A., (2015). Removal of cyanide from aqueous solutions by adsorption on activated carbon prepared from lignocellulosic by-products. J. Dispersion Sci. Technol., 36(12): 1736-1741 **(6 pages)**.

Hirabayashi, D.; Yoshikawa, T.; Kawamoto, Y.; Mochizuchi, K.; Suzuki, K., (2006). Characterization and applications of calcium ferrites based materials containing active oxygen species. Adv. Sci. Tech. 45: 2169-2175 **(7 pages)**.

Hung, D.; Thanh, N., (2011). Preparation of NiFe2O4 - TiO2 nanoparticles and study of their photocatalytic activity. J. Math. Phys. 27(4): 204-211 **(8 pages)**.

Kadi, M.; Mohamed, R., (2015). Environmental Remediation of Aqueous Cyanide by Photocatalytic Oxidation using a NiFe2O4/TiO2-SiO2 Core-Shell Nanocomposite. Desalin. Water Treat. 56(7): 1940-1948 **(9 pages)**.

Kadi, M.W.; Mohamed, R.M., (2014). Synthesis and optimization of cubic NiFe2O4 nanoparticles with enhanced saturation magnetization. Ceram. Int., 40(1): 227-232 **(6 pages)**.

Kariim, I.; Abdulkareem, A.S.; Tijani, J.O.; Abubakre, O.K., (2020). Development of MWCNTs/TiO2 nanoadsorbent for Simultaneous removal of Phenol and Cyanide from refinery wastewater. Scientific African, e00593.

Kaušpėdienė, D.; Gefenienė, A.; Ragauskas, R.; Pakštas, V. (2017). Comparative investigation of plain and silver impregnated activated carbons for the removal of cyanide from basic aqueous solutions in the batch process. Chem. Eng. Commun., 204(11): 1258-1269 **(12 pages)**.

Kuo, Y.; Hsu, W.; Chiu, P.; Tseng, Y.; Ku, Y., (2013). Assessment of redox behaviour of nickel ferrite as oxygen carriers for chemical looping process. Ceram. Int., 39: 5459-5465 **(7 pages)**.

Kuyucak, N.; Akcil, A., (2013). Cyanide and removal options from effluents in gold mining and metallurgical processes. Miner. Eng., 50: 13-29 **(17 pages).**

Li, S.; Han, K.; Li, J.; Li, M.; Lu, C., (2017). Preparation and characterization of super activated carbon produced from gulfweed by KOH activation. Microporous Mesoporous Mater., 243: 291-300 **(10 pages).**

Livani, M.J.; Ghorbani, M. ; Mehdipour, H., (2018). Preparation of an activated carbon from hazelnut shells and its hybrids with magnetic NiFe2O4 nanoparticles. New Carbon Mater., 33(6): 578-586 **(7 pages).**

Manova, E.; Tsoncheva, T.; Paneva, D.; Popova, M. ; Velinov, N.; Kunev, B.; Mitov, I., (2011). Nanosized copper ferrite materials: Mechanochemical synthesis and characterization. J. Solid State Chem. 184(5): 1153-1158 **(6 pages)**.

Marsden, J.O.; House, C.L., (2006). The chemistry of gold extraction. 2nd. Ed. Society for mining, metallurgy and exploration Inc.

Mudarra, J., (2017). Efecto del carbón activado de la cáscara de coco, reforzado con iones cúpricos pentahidratados, en la remoción de cianuro acuoso. Cientifi-k, 5(1): 47-54 **(8 pages)**.

O'Driscoll, B.; Clay, P.; Cawthorn, R.; Lenaz, D.; Adetunji, J.; Kronz, A., (2014). Trevorite: Ni-rich spinel formed by metasomatism and desulfurization processes at Bon Accord, South Africa? Mineral. Mag. 78(1): 145-163 **(19 pages)**.

Pesántez, D.; De la Torre, E.; Guevara, A., (2010). Influencia del ion cúprico y del cobre metálico en la oxidación del cianuro libre con aire y carbón activado. Revista Politécnica, 29(1): 1-7 **(7 pages)**.

Rafique, M. Y.; Ellahi, M.; Iqbal, M. Z.; Pan, L., (2016). Gram scale synthesis of single crystalline nano-octahedron of NiFe2O4: Magnetic and optical properties. Mater. Lett., 162: 269-272 **(4 pages)**.

Rojas, N.; Bustamante, M., (2007). Copper dissolution from cupric ferrite in conventional cyanidation. Dyna-Colombia, 74(152): 151-157 **(7 pages)**.

Singh, N.; Balomajumder, C., (2016). Simultaneous removal of phenol and cyanide from aqueous solution by adsorption onto surface modified activated carbon prepared from coconut shell. J. Water Process Eng., 9: 233-245 **(13 pages).**

Sivakumar, D., (2015). Hexavalent chromium removal in a tannery industry wastewater using rice husk silica. Global J. Environ. Sci. Manage., 1(1): 27-40 **(14 pages)**.

Stavropoulos, G.; Skodras, G.; Papadimitriou, K., (2013). Effect of solution chemistry on cyanide adsorption in activated carbon. Appl. Therm. Eng., 74: 182-185 **(4 pages)**.

Stoyanova, M.; Christoskova, S., (2005). Novel Ni-Fe-oxide systems for catalytic oxidation of cyanide in an aqueous phase. Central Europ. Sci. J., 3(2): 295-310 **(6 pages)**.

Teixeira, L.; Arellano, M.; Sarmiento, C.; Yokoyama, L.; Fonseca, F., (2013a). Oxidation of cyanide in water by singlet oxygen generated by the reaction between hydrogen peroxide and hypochlorite. Mineral. Eng., 50: 57-63 **(7 pages)**.

Teixeira, L.; Andia, J.; Yokoyama, L.; Fonseca, F.; Sarmiento, C., (2013b). Oxidation of cyanide in effluents by Caro's Acid. Mineral. Eng., 45: 81-87 **(7 pages).**

Tian, S.; Li, Y.; Zhao, X., (2015). Cyanide removal with a copper/active carbon fiber cathode via a combined oxidation of a Fenton-like reaction and in situ generated copper oxides at anode. Electrochim. Acta, 180: 746-755 **(10 pages)**.

Zandipak, R.; Sobhanardakani, S., (2016). Synthesis of NiFe2O4 nanoparticles for removal of anionic dyes from aqueous solution. Desalin. Water Treat. 57(24): 11348-11360 **(13 pages)**.

Zhao, Q.; Yan, Z.; Chen, C.; Chen, J., (2017). Spinels: Controlled preparation, oxygen reduction/evolution reaction application, and beyond. Chem. Rev., 117(15): 10121-10211 **(91 pages)**.

AUTHOR (S) BIOSKETCHES

Feijoo, C.Y., M.Sc., Researcher, Department of Extractive Metallurgy, Escuela Politécnica Nacional, Ladrón de Guevara, Quito 170517, Ecuador, and Instituto de Investigación Geológico y Energético, Quito, Ecuador. Email: *cristhian.feijoo@epn.edu.ec*

De la Torre, E., Ph.D., Professor, Department of Extractive Metallurgy, Escuela Politécnica Nacional, Ladrón de Guevara, Quito 170517, Ecuador. Email: *ernesto.delatorre@epn.edu.ec*

Narváez, R.A.C., Ph.D., Professor, Instituto de Investigación Geológico y Energético, Quito, Ecuador, and Universidad Central del Ecuador, UCE-GIIP, EC170521, Quito, Ecuador. Email: *ricardo.narvaez@geoenergia.gob.ec*